AIP | Applied Physics Letters

Acoustic cloaking by a near-zero-index phononic crystal

Li-Yang Zheng, Ying Wu, Xu Ni, Ze-Guo Chen, Ming-Hui Lu, and Yan-Feng Chen

Citation: Applied Physics Letters **104**, 161904 (2014); doi: 10.1063/1.4873354
View online: http://dx.doi.org/10.1063/1.4873354
View Table of Contents: http://scitation.aip.org/content/aip/journal/apl/104/16?ver=pdfcov
Published by the AIP Publishing

Acoustic cloaking by a near-zero-index phononic crystal

Li-Yang Zheng,[1] Ying Wu,[2] Xu Ni,[1] Ze-Guo Chen,[1] Ming-Hui Lu,[1,a)] and Yan-Feng Chen[1]
[1]*National Laboratory of Solid State Microstructures and Department of Materials Science and Engineering, Nanjing University, Nanjing 210093, China*
[2]*Computer, Electrical and Mathematical Sciences and Engineering, King Abdullah University of Science and Technology (KAUST), Thuwal 23955-6900, Saudi Arabia*

(Received 11 March 2014; accepted 14 April 2014; published online 22 April 2014)

Zero-refractive-index materials may lead to promising applications in various fields. Here, we design and fabricate a near Zero-Refractive-Index (ZRI) material using a phononic crystal (PC) composed of a square array of densely packed square iron rods in air. The dispersion relation exhibits a nearly flat band across the Brillouin zone at the reduced frequency $f = 0.5443c/a$, which is due to Fabry-Perot (FP) resonance. By using a retrieval method, we find that both the effective mass density and the reciprocal of the effective bulk modulus are close to zero at frequencies near the flat band. We also propose an equivalent tube network model to explain the mechanisms of the near ZRI effect. This FP-resonance-induced near ZRI material offers intriguing wave manipulation properties. We demonstrate both numerically and experimentally its ability to shield a scattering obstacle and guide acoustic waves through a bent structure. © *2014 AIP Publishing LLC*. [http://dx.doi.org/10.1063/1.4873354]

Zero-refractive-index (ZRI) materials are unconventional materials that exhibit zero refractive indices.[1–14] In a ZRI material, waves do not experience spatial phase changes, because the phase velocity, inversely proportional to the refractive index, approaches infinity and the wavelength becomes very long even at high frequencies.[1] This special characteristic enables unprecedented wave properties, such as tunneling of electromagnetic energy through sub-wavelength channels and bend,[2] tailoring of the radiation phase pattern of electromagnetic sources,[3] and super-reflection or cloaking with different defect loadings.[4–7] In electromagnetic wave propagation, according to the relationship that the refractive index is directly related to the permittivity, ε, and permeability, μ, via $n = \sqrt{\varepsilon\mu}$, two kinds of ZRI materials are categorized: (I) single-zero-index materials, in which only one parameter is zero. One such material, known as the epsilon-near-zero (ENZ) material, can be achieved by utilizing metamaterials,[7,8] plasma,[9] and metal-clad waveguides.[1] However, this strategy depends heavily on a few specific plasmonic materials or complex metamaterials. (II) double-zero-index (DZI) materials, with two parameters being zero simultaneously. There are two ways to achieve a DZI material in electromagnetics: One is to achieve matched zero-index material by embedding resonant non-magnetic inclusions into an ENZ host medium.[10] The other is to utilize a photonic crystal possessing a Dirac-like cone inducted by accidental degeneracy, at which the effective permittivity and permeability are zero simultaneously.[11]

The acoustic analog of ZRI materials has also been explored extensively. For instance, by installing thin tensioned circular membranes to the rigid plane perforated with subwavelength holes, one can make the mass of the air in the holes effectively vanish because the restoring force from the membrane adds a negative term to the effective mass.[12] The design suits better for extraordinary acoustic transmission, but applications on cloaking have seldom been reported. Another example is the acoustic analogy of the electromagnetic DZI material, in which the effective mass density and the reciprocal of the effective bulk modulus vanish simultaneously at the Dirac-like point.[13,14] Although the problem for acoustic waves can be mapped from its electromagnetic counterpart mathematically, the requirement on low wave velocity in the inclusions greatly limits the application of zero-index materials in airborne sound. This limitation may be overcome due to the rapid progress in metamaterials.[15–24]

In this work, we propose a simple method to achieve near zero quantities in both the effective mass density and the reciprocal of the effective bulk modulus for airborne sound in a 2D phononic crystal (PC). Different from the previous approaches,[7–11] no materials with extreme material parameters are required, and the near-zero effective medium parameters come from the zeroth order Fabry-Perot (FP) resonance which exhibits an infinite phase velocity. We numerically and experimentally demonstrated that the phononic crystal can hide an obstacle. This FP resonance induced cloaking effect is fundamentally different from transformation acoustics[25,26] or scattering cancelation.[27,28] We also experimentally observe the bending effect that sound wave can pass through a bend waveguide with our PC embedded in it.

The 2D PC considered in this study is composed of a square array of square steel rods in air. A schematic of the structure, with four units, is shown in the inset of Fig. 1(a). The dimension of the steel rod is infinite along Z direction. While in X and Y directions, the steel rod has the same size of $l = 0.89a$, where a is the lattice constant. The mass densities of steel and air are $\rho = 7870\,\mathrm{kg/m^3}$ and $\rho_0 = 1.25\,\mathrm{kg/m^3}$, respectively, and their corresponding sound velocities are $c = 5960\,\mathrm{m/s}$ and $c_0 = 343\,\mathrm{m/s}$. Fig. 1(a) shows the band structure of the PC calculated by COMSOL Multiphysics, a finite-element-based commercial software capable of full-wave simulations.

a)Author to whom correspondence should be addressed. Electronic mail: luminghui@nju.edu.cn.

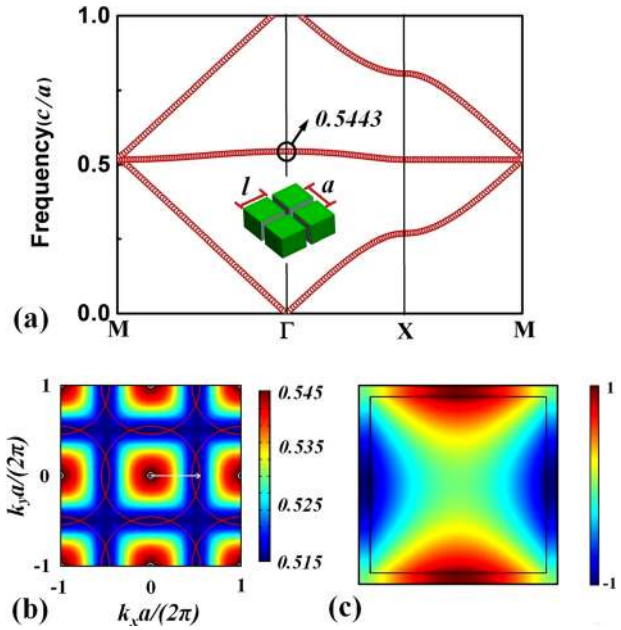

FIG. 1. (a) The band structure of the PC. A flat band is noticed around $f=0.544c/a$. The inset is a schematic of the PC structure. A square array of square steel rods of the same size, l, are placed in air with the lattice constant a. (b) The IFCs of the flat band. At the working frequency, IFC is a small circle noted as blue line. The red circle represents the IFC of air. (c) The pressure field pattern of one unit cell at $f=0.5443c/a$.

Apparent in Fig. 1(a) is a flat branch, near the frequency of $0.5c/a$ and across the whole Brillouin zone, that does not intersect with any other branches.

Field distribution of the eigenmode on the flat branch at the Γ point is plotted in Fig. 1(c). Due to the large impedance mismatch between steel and air, the acoustic wave field is mainly concentrated in the narrow air channels. To better understand the underlying physics, the iso-frequency contour (IFC) of the flat band is analyzed. As shown in Fig. 1(b), the IFC is nearly circular in the vicinity of the Γ point, while it becomes more rectangular when the frequency decreases. But at the working frequency $0.5443c/a$, the IFC is a small circle (blue line). It indicates that the phononic crystal can be regarded as an isotropic effective medium at that frequency. Therefore, to better understand the interaction of sound waves in the interfaces, we can use its effective medium parameters to describe the wave propagation.

Near the center of the Brillouin zone, the system may be characterized by an effective medium theory (EMT) because $\vec{k}$ is almost zero.[29] Here, the effective mass density, ρ_{eff} and bulk modulus, B_{eff}, are calculated from the transmission and reflection coefficients,[30] denoted as T and R, respectively, of a plane wave normally incident on a finite-sized slab of the PC evaluated by COMSOL. The results of ρ_{eff} and $1/B_{eff}$ are plotted in Fig. 2(b) as blue and red solid curves, respectively. This figure shows that both the effective mass density and reciprocal of bulk modulus undergo a jump near the frequency of $0.5437c/a$. Though the reciprocal of the effective bulk modulus is negative and very close to zero in this frequency regime, the effective mass density varies drastically from positive value to a negative one. It then gradually increases and becomes positive again. When the frequency reaches $f=0.5443c/a$, $\rho_{eff}=0$. Both of the effective parameters are

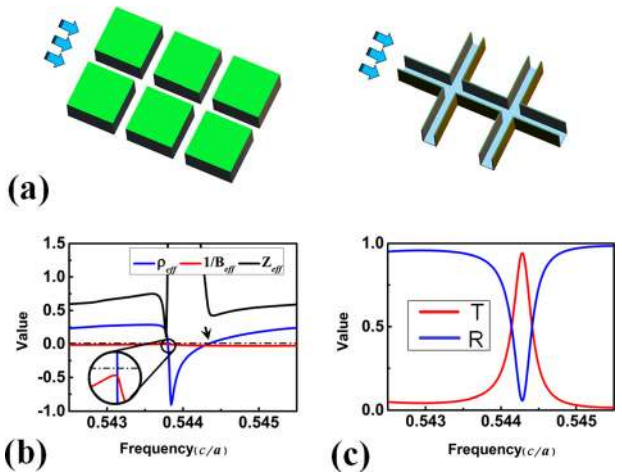

FIG. 2. (a) An equivalent tube network model of the PC. (b) Effective medium parameters of the PC. The effective mass density and reciprocal of bulk modulus undergo a drastic change near the frequency of $0.5437c/a$. Then, the effective mass density gradually increases as the frequency increases. At $f=0.5443c/a$, it equals zero. (c) The transmittance (reflectance) changes as the frequency increases. The transmittance comes to a peak value (roughly 0.8) at $0.5443c/a$.

negative between frequencies $0.5437c/a$ and $0.5443c/a$, which implies that there is a negative band within this narrow frequency regime.

To explain the mechanisms of near zero mass density and reciprocal of bulk modulus, we propose an equivalent tube network model, shown in Fig. 2(a), of the PC. The PC in this work is constructed by square steel rods embedded in air background with a high filling ratio of 0.79. It leads to a sub-wavelength air channel between two adjacent steel unit cells. Considering the rigidness of steel cells, which can be treated as hard boundary, the sub-wavelength air channel is equivalent to a sub-wavelength short tube. As the number of the steel rod layers increases along the propagating direction, it is similar to the case when we put many identical short tubes in series. From this perspective, the whole PC can be viewed as a sub-wavelength tube network. For each short horizontal tube along the propagating direction, the vibration velocity will be generated as the air in the internal hollow FP cavity vibrates back and forth. At resonant frequency, large amount of energy is stored in the internal cavity, which causes the acceleration of the air medium in the opposite direction of the excited sound pressure and induces the negative effective mass density. On the other hand, the tube network also has vertical sub-wavelength tubes which are perpendicular to the propagation direction. These vertical tubes have the same size of the horizontal ones and can lead to negative effective bulk modulus at resonant frequencies because the air in the horizontal channels can flow in and out of the vertical tubes when pressure is imposed. Fundamentally, the principle is similar to the previously investigated acoustic systems consisting of arrays of side-attached tubes, Helmholtz resonators, in which closed cavities are connected to the channel.[21,31] Although the vertical tubes in this model are opened cavities, they still serve similar purpose as the Helmholtz resonators did because this two kinds of cavities in the side-attached cases act as the role to store wave energy and cause vibrations when sound wave is applied

From this tube network model, there are two kinds of tubes, the horizontal ones, which provide negative effective mass density, and the vertical ones, which can change effective bulk modulus, interacting together at resonant frequency $0.5437c/a$ to open a negative band for propagation of sound wave. Due to the identical sizes of all the tubes, resonance occur at the same frequency of $0.5437c/a$, leading to both effective mass density and bulk modulus undergo a sharp drop simultaneously (leap for the reciprocal of the effective bulk modulus as shown in Fig. 2(b)). When working frequency increases, effective mass density varies gradually and comes to zero at $0.5443c/a$. Near this frequency, propagation of sound wave is still permitted, while both effective mass density and reciprocal of bulk modulus are very close to zero, leading to the fantastic phenomenon of ZRI.

A ZRI material can give rise to various intriguing phenomena such as cloaking and beam-shaping.[1,11] Here, we demonstrate in both simulations and experiments the cloaking of an object by the PC. The experimental set-up is shown in Fig. 3(a), which exhibits an obstacle made of a steel block of size $4a \times 2a$ (red rectangle) and is embedded in the PC containing 10×8 steel rods(green) with the lattice constant $a = 4.5$ mm. The waveguide was constructed by sponges (yellow) located at four sides of the PC that can minimize reflections. We used a Function Generator (Agilent 33120A 15 MHz Function Waveform Generator) as sound source and an ultrasonic transducer, whose central frequency is 40 kHz, attached closely to the waveguide port to generate the incident wave (working frequency in the experiment is 39.1 kHz). We placed the transducer 100 mm away from the left side of the PC to mimic a good plane wave source in the sponge waveguide. A Brüel & Kjær free field 1/8 Inch microphone (Brüel & Kjær Type 2670) is placed 45 mm away from the right side of the PC to detect the sound wave. The phase and amplitude of sound waves are recorded by the oscilloscope (Zolix DPO 2012) and the lock-in amplifier (EG&G MODEL 5302 Lock-in Amplifier). With the help of computer, experimental data then can be postprocessed. In this work, sound waves were incoming normally to the sample; thus, we do not have to consider multiple reflections in the waveguide.

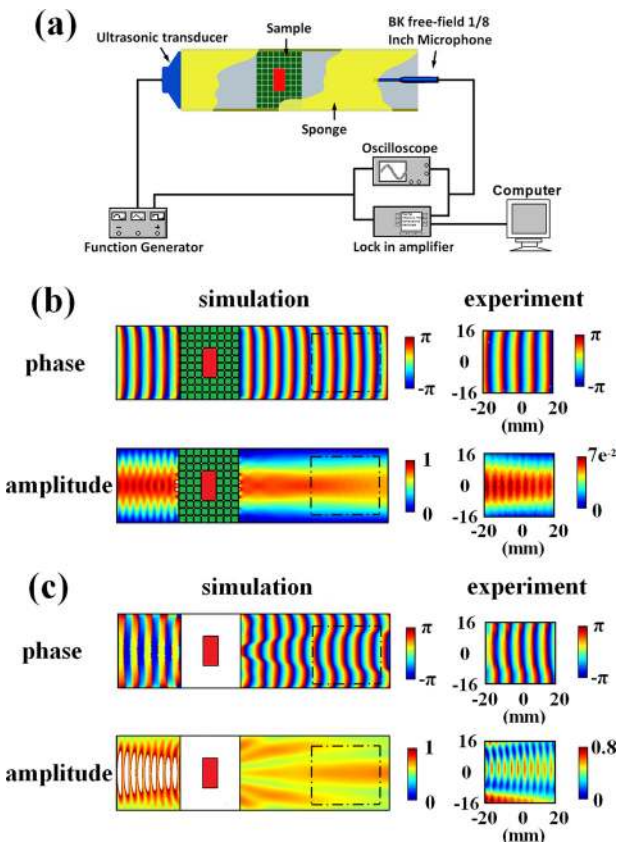

FIG. 3. (a) Schematics of the experimental setup used to map the sound field behind the sample. The phase and normalized amplitude patterns with (b) and without (c) the PC in the waveguide. Left: simulated result. Right: the experimental result for the region corresponding to the dashed box shown in left. Note that there exist some white areas in the amplitude patterns in simulations. It means that the amplitude is larger than 1.

The normalized pressure field and the phase pattern of a 32×40 mm^2 area in the detection area are shown in the right panel of Fig. 3(b). In the experiment, acoustic waves with frequencies of $0.513c/a$ (39.1 kHz) was incoming from the left and impinging on the PC containing the obstacle. The simulation is also shown in the left panel of Fig. 3(b), where the operating frequency $0.545c/a$ (41.54 kHz) is slightly higher than $0.5443c/a$ (41.47 kHz) due to the small change in the impedance when obstacle is embedded in the PC. Despite the imperfection from the plane wave source and boundary reflections, it is obvious that the wave front preserves its original pattern after it passes through the PC as if the steel block was not there. The measured results agree well with the simulation. For comparison, the simulated and measured results for the case when the PC is removed and the steel block remains are plotted in Fig. 3(c). A clear shadow cast by the steel block and a distorted wavefront can be observed in both figures, suggesting that the cloaking effect shown in Fig. 3(c) does not exist. The PC therefore plays a crucial role in hiding the object inside a waveguide channel.

The transmittance of the PC-based ZRI material in this work is high for a lossless system (shown in Fig. 2(c)). But in the experiment, we observed the cloaking effect at $0.513c/a$ and the transmittance was only about 2% (shown in Fig. 4(b)), which implies that the attenuation is big, and the transmittance is small. Theoretically, a perfect flat band leads to large attenuation.[32,33] In particular, loss becomes much more complicated at working frequency when strong FP resonance occurs. Therefore, although sound waves still can travel through the PC, the loss leads to a significant decrease

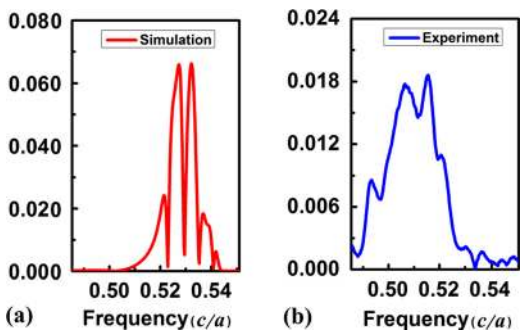

FIG. 4. The transmission of sound waves when loss was taken into account. (a) Theoretical (red curve) and (b) experimental (blue curve) pressure intensity transmission spectra with PC and the obstacle in the waveguide.

in the transmittance and a shift of the working frequency for cloaking effect. This phenomenon can be easily verified in both theory and experiment as shown in Fig. 4. For simplicity, only the viscous force of air in the narrow channel was considered in calculation and the calculated transmittance of attenuation coefficient $\alpha = 8.16$ is shown in Fig. 4(a), which demonstrate a shift in the transmission peaks and a drop in the amplitudes. Comparing the experiment result (Fig. 4(b)) with the calculation, we can see that number of peaks and the profile of transmittance are consistent with each other. It implies that losses would reduce the transmission amplitudes and lead to a shift of the working frequency. However, it would not change the physical phenomenon. Thus, we can extend this idea to small loss system such as water sound. Since loss in water is much smaller than that in air, transmittance will increase largely and the cloaking effect will be much more perfect.

Another fascinating property of our PC-based ZRI material is shown in Fig. 5, which demonstrates that waves can pass through a bent waveguide with an object embedded in the PC. Fig. 5(a) shows a cutaway view of the experimental set up, where the same PC and the same steel block as shown in Fig. 3(a) are used and the walls of the bent waveguide are again made of sponge. The plane waves at the frequency of $0.513c/a$ is incident on the PC from the lower left channel; they turn through the 90° end in the PC channel; they then exit from the upper right channel. The simulated and measured phase and amplitude patterns are shown in Fig. 5(b). Although there are slight distortions, the main features of the incident plane wave are preserved. Thus, the bending of acoustic waves is achieved with the PC and the cloaking effect is also realized. The steel object inside the PC does not distort the plane wave front after sound waves pass through the PC, creating the illusion that the object is not there. The phase and amplitude patterns for the case without the PC are shown in Fig. 5(c). It can be seen that plane wave front does not exist at the upper right channel.

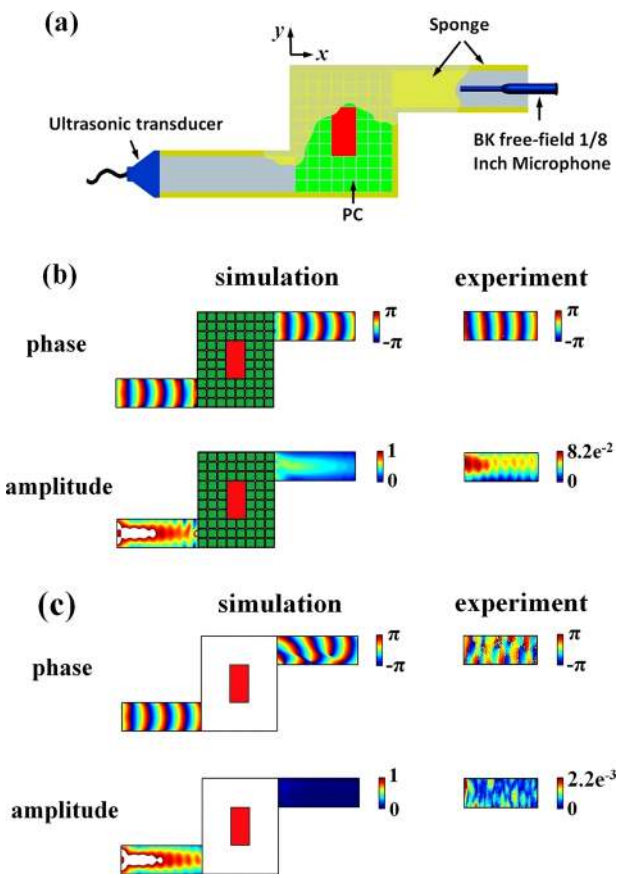

FIG. 5. Numerical and experimental demonstrations of the bending effect. (a) A sketch of the same configurations as shown in Fig. 3(a). The incident wave comes from the lower left channel and the phase pattern at the upper right channel is measured by the scanning detector. Simulated and experimental phase and normalized amplitude patterns with (b) and without (c) the PC in the waveguide.

In conclusion, different from the previously studied ZRI materials, we have theoretically designed and experimentally fabricated a phononic-crystal-based ZRI material. The PC consists of closely packed identical square steel rods. It exhibits the peculiar dispersion characteristic of a flat branch across the Brillouin zone near $f = 0.5443c/a$. The physical origin of this flat band is the zeroth order FP resonance, which gives rise to the infinite phase velocity in the air channels. It ensures no phase change when sound waves pass through the PC. Consequently, the PC exhibits an effective ZRI. This FP-induced ZRI material also offers unprecedented wave properties. We explicitly illustrate, through numerical simulation and experiments, its abilities to shield an object and guide waves through a bent structure. There are many possible applications for this easily fabricated PC in manipulating acoustic waves through ZRI materials.

This work was jointly supported by the National Basic Research Program of China (Grant Nos. 2012CB921503 and 2013CB632904) and the National Natural Science Foundation of China (Grant No. 1134006). We also acknowledge the Academic Development Program of Jiangsu Higher Education (PAPD) and KAUST Baseline Research Funds.

[1]N. Engheta, Science **340**, 286 (2013).
[2]M. G. Silveirinha and N. Engheta, Phys. Rev. B **76**, 245109 (2007).
[3]A. Alù, M. G. Silveirinha, A. Salandrino, and N. Engheta, Phys. Rev. B **75**, 155410 (2007).
[4]V. C. Nguyen, L. Chen, and K. Halterman, Phys. Rev. Lett. **105**, 233908 (2010).
[5]J. Hao, W. Yan, and M. Qiu, Appl. Phys. Lett. **96**, 101109 (2010).
[6]Y. Xu and H. Chen, Appl. Phys. Lett. **98**, 113501 (2011).
[7]Y. Wu and J. Li, Appl. Phys. Lett. **102**, 183105 (2013).
[8]R. Liu, Q. Cheng, T. Hand, J. J. Mock, T. J. Cui, S. A. Cummer, and D. R. Smith, Phys. Rev. Lett. **100**, 023903 (2008).
[9]E. J. R. Vesseur, T. Coenen, H. Caglayan, N. Engheta, and A. Polman, Phys. Rev. Lett. **110**, 013902 (2013).
[10]M. Silveirinha and N. Engheta, Phys. Rev. B **75**, 075119 (2007).
[11]X. Huang, Y. Lai, Z. H. Hang, H. Zheng, and C. T. Chan, Nature Mater. **10**, 582 (2011).
[12]J. J. Park, K. J. B. Lee, O. B. Wright, M. K. Jung, and S. H. Lee, Phys. Rev. Lett. **110**, 244302 (2013).
[13]F. Liu, X. Huang, and C. T. Chan, Appl. Phys. Lett. **100**, 071911 (2012).
[14]F. Liu, Y. Lai, X. Huang, and C. T. Chan, Phys. Rev. B **84**, 224113 (2011).
[15]Z. Liang and J. Li, Phys. Rev. Lett. **108**, 114301 (2012).
[16]H. Estrada, P. Candelas, F. Belmar, A. Uris, J. Garcia de Abajo, and F. Meseguer, Phys. Rev. B **85**, 174301 (2012).
[17]J. Christensen and F. Javier Garcia de Abajo, Phys. Rev. Lett. **108**, 124301 (2012).
[18]Z. Liu, C. T. Chan, and P. Sheng, Phys. Rev. B **62**, 2446–2457 (2000).
[19]Y. Cui, K. H. Fung, J. Xu, H. Ma, J. Yi, S. He, and N. X. Fang, Nano Lett. **12**, 1443 (2012).

[20]J. Zhu, Y. Chen, X. Zhu, F. J. Garcia-Vidal, X. Yin, W. Zhang, and X. Zhang, Sci. Rep. **3**, 1728 (2013).
[21]K. J. B. Lee, M. K. Jung, and S. H. Lee, Phys. Rev. B **86**, 184302 (2012).
[22]S. Yang, J. H. Page, Z. Liu, M. L. Cowan, C. T. Chan, and P. Sheng, Phys. Rev. Lett. **93**, 024301 (2004).
[23]C. Goffaux and J. P. Vigneron, Phys. Rev. B **64**, 075118 (2001).
[24]Z. Liu, X. Zhang, Y. Mao, Y. Y. Zhu, Z. Yang, C. T. Chan, and P. Sheng, Science **289**, 1734–1736 (2000).
[25]S. Zhang, C. Xia, and N. Fang, Phys. Rev. Lett. **106**, 024301 (2011).
[26]N. Stenger, M. Wilhelm, and M. Wegener, Phys. Rev. Lett. **108**, 014301(2012).
[27]S. A. Cummer, B. I. Popa, D. Schurig, D. R. Smith, J. Pendry, M. Rahm, and A. Starr, Phys. Rev. Lett. **100**, 024301 (2008).
[28]L. Sanchis, V. M. García-Chocano, R. Llopis-Pontíveros, A. Climente, J. Martínez-Pastor, F. Cervera, and J. Sánchez-Dehesa, Phys. Rev. Lett. **110**(12), 124301 (2013).
[29]Y. Wu, J. Li, Z. Q. Zhang, and C. T. Chan, Phys. Rev. B **74**, 085111 (2006).
[30]V. Fokin, M. Ambati, C. Sun, and X. Zhang, Phys. Rev. B **76**, 144302 (2007).
[31]N. Fang, D. J. Xi, J. Y. Xu, M. Ambati, W. Srituravanich, C. Sun, and X. Zhang, Nature Mater. **5**, 452 (2006).
[32]E. N. Economou and M. Sigala, J. Acoust. Soc. Am. **95**(4), 001734 (1994).
[33]J. V. Sánchez-Pérez, D. Caballero, R. Mártinez-Sala, C. Rubio, J. Sánchez-Dehesa, F. Meseguer, J. Llinares, and F. Gálvez, Phys. Rev. Lett. **80**, 5325–5328 (1998).